Aerosol Flame Synthesis and Manipulating Upconversion Luminescence of Ultrasmall Y_2O_3:Yb^{3+}/Ho^{3+} Nanoparticles

Shuai Hu, Maohui Yuan, Linxuan Wang, Changqing Song, Zining Yang, Hongyan Wang, and Kai Han

***Abstract*—The synthesis of upconversion nanoparticles (UCNPs) by flame aerosol is of great significance to realize industrial large-scale production of UCNPs and develop nanotechnology further. Here, for the first time, we successfully fabricated the ultrasmall Y_2O_3:Yb^{3+}/Ho^{3+} UCNPs by a self-build swirl flame spray pyrolysis (SFSP) method with a high production rate of ∼40 g·h^{-1}. These flame-made UCNPs are all pure cubic phases with an average ultrasmall size of ∼14 nm. Excited by 980 nm laser, the synthesized UCNPs show bright green ($^2F_4$, $^5S_2 \rightarrow {}^5I_8$) and relatively weak red ($^5F_5 \rightarrow {}^5I_8$) upconversion luminescence (UCL). Based on the UCL spectra of Y_2O_3:Yb^{3+}/Ho^{3+} UCNPs, the optimal doping concentrations of 6 mol% Yb^{3+} and 0.1 mol% Ho^{3+} were determined to reach the most intense UCL. The dependence of UCL intensity and pump power was further analyzed, and it indicated that the green and red UCL are two-photon processes. In addition, the UCL properties with different synthesized conditions were also demonstrated. The UCL mechanism of these flame-made Y_2O_3:Yb^{3+}/Ho^{3+} UCNPs were illustrated in detail. Our results prove that industrial large-scale production of continuous one-step synthesis of UCNPs by flame aerosol technology is completely feasible and deserves further study.**

***Index Terms*—Photonic materials, synthesis and fabrication methods, luminiescence and fluorescence, optical properties of photonic materials.**

I. Introduction

UCNPs refer to the lanthanide-doped nanoparticles that can harvest and convert near-infrared low-energy photons into visible or ultraviolet high-energy photons to realize photon upconversion (UC), which are of broad applications in the fields of three-dimensional display, anti-counterfeiting, laser materials, sensors, biological issues, and photovoltaics [1], [2]. Generally, the strategies of synthesizing UCNPs mainly focus on wet chemical routes, including hydrothermal [3]–[5], sol-gel [6]–[8], co-precipitation [9]–[11], thermal decomposition [12]–[14] and ion exchange method [15], [16]. Moreover, some newly emerging methods, such as laser ablation [17], [18], solid state reaction [19]–[22], and electrospinning [23], [24] are also used for fabricating the UCNPs. However, the UCNPs fabricated by these routes are always accompanied by complex chemical processes and harsh experimental conditions. In terms of the traditional wet chemical method, the fabricated particles always need further treatment like separation or drying, which not only take times but also stop the continuous production of UCNPs so that unfit the reuirements of industrial production. Instead, the flame method can realize the rapid, one-step and continuous preparation of UCNPs, which fabricates UCNPs in seconds while keeping supply of precursors that exactly fitting the mass continuous production requirement of industry and can further promote the applications of nanotechnology in UCNPs field. Otherwise, the liquid-feed flame aerosol method is easy to realize automatic production for that the supply of fuel, oxidant and precursor can be controlled through simple electronic circuit systems and programs. The flame synthesis has been successfully used in industry for several decades to manufacture nanoparticles like carbon black, silica, alumina, and titania with large-scale production, and the current production rate can reach up to as large as 25 tons per hour [25]–[27]. Thus, the flame aerosol technology can be potentially used to realize commercial mass production of UCNPs, which will efficiently facilitate its applications. However, rare efforts are made to conduct the synthesis of UCNPs with flame aerosol technology.

Generally, the UCNPs are composed of inorganic matrix and doping with appropriate rare-earth-ions [1], which has been successfully demonstrated in Y_2O_3 [10], [28]–[31], $NaYF_4$ [32], $LiYF_4$ [33], YVO_4 [34], CaF_2 [4] hosts. In these compounds, Y_2O_3 is a typical UC matrix due to its outstanding characters such as large bandgap (∼5.8 eV), wide spectral range in optical transparency (0.2∼8 μm), high refractive index (∼2), low phonon energy (∼600 cm^{-1}), high breakdown strength, excellent thermal stability and electronic properties [10], [35], [36]. Moreover, the radius of Y^{3+} ions is equivalent to those doped target rare-earth-ions, which is beneficial to reduce the influence of doping on the matrix lattice structure, further reduce lattice impurities and improve the UCL intensity [1], [10].

Manuscript received December 20, 2021; revised January 30, 2022; accepted February 7, 2022. Date of publication February 11, 2022; date of current version March 4, 2022. *(Corresponding authors: Changqing Song; Kai Han.)*

Shuai Hu, Linxuan Wang, Changqing Song, Zining Yang, and Hongyan Wang are with the Hunan Provincial Key Laboratory of High Energy Laser Technology, College of Advanced Interdisciplinary Studies, National University of Defense Technology, Changsha, Hunan 410073, China (e-mail: hushuai0015@163.com; wlx941781132@163.com; songchangqing08@nudt.edu.cn; yangzining09@nudt.edu.cn; wanghongyan@nudt.edu.cn).

Maohui Yuan is with the College of Advanced Interdisciplinary Studies, National University of Defense Technology, Changsha, Hunan 410073, China, and also with the Department of Physics and Chemistry, PLA Army Academy of Special Operations, Guangzhou, Guangdong 510507, China (e-mail: yuanmaohuino1@126.com).

Kai Han is with the State Key Laboratory of Pulsed Power Laser Technology, College of Advanced Interdisciplinary Studies, National University of Defense Technology, Changsha, Hunan 410073, China (e-mail: hankai0071@nudt.edu.cn).

Digital Object Identifier 10.1109/JPHOT.2022.3150524

Consequently, Y_2O_3 is a suitable candidate matrix for the flame synthesis of UCNPs. To enhance the UCL efficiency, UCNPs are usually doped with two different kinds of rare-earth-ions based on the mechanism of sensitization and activation. Yb^{3+}/Ho^{3+} co-doped nanomaterial is one of the most common systems that can achieve efficient UCL owing to the highly resonant energy-transfer between the sensitizer Yb^{3+} and activator Ho^{3+} ions. Under the 980 nm laser excitation, the Yb^{3+}/Ho^{3+} co-doped UCNPs usually emit bright green ($^2F_4$, $^5S_2 \rightarrow {}^5I_8$) and relatively weak red ($^5F_5 \rightarrow {}^5I_8$) UC emissions [1], [10], [29], [30], [37]. However, up to now, there are so few related report demonstrated on the flame-made Yb^{3+}/Ho^{3+} co-doped UCNPs, leading to their UCL properties remaining also unclear. Thus, it is of great necessary to conduct Y_2O_3:Yb^{3+}/Ho^{3+} UCNPs synthesis experiment by the flame aerosol technology.

In this work, for the first time, we fabricated the ultrasmall Y_2O_3:Yb^{3+}/Ho^{3+} UCNPs by a self-build swirl-stabilized spray flame reactor, confirming that as a rapid continuous one-step method for synthesis of UCNPs with a high production rate. Furthermore, their structural and UCL properties were also systematically investigated in detail, which verifies that both the Yb^{3+} and Ho^{3+} ions are successfully incorporated in the Y_2O_3 matrix and exhibit intense UCL. In addition, the power dependence on UCL intensity, impact of synthesis conditions and the mechanism of the UCL are also discussed to further support the observed experimental results.

II. Experimental

A. Raw Materials

The chemicals involved in this paper were purchased from Aladdin Industrial Corporation including $Y(NO)_3{\cdot}6H_2O$ (99.9%), $Yb(NO)_3{\cdot}5H_2O$ (99.9%), $Ho(NO)_3{\cdot}5H_2O$ (99.99%), n-Butanol (99%) and 2-Ethylhexanoic acid (2-EHA) (>99%). All chemicals were not further purified.

B. Synthesis of Y_2O_3:Yb^{3+}/Ho^{3+} UCNPs by Swirl-Stabilized Flame

To prepare Y_2O_3:Yb^{3+}/Ho^{3+} UCNPs, we first have to configure the precursor with the right rare-earth-ion concentrations. The required chemicals were weighed according to the precalculated stoichiometric ratio, then mixed and dissolved in n-butanol. 2-EHA were added into the mixed n-butanol solution next for replacing nitrate ions, so that the precursor can volatilize better in the reaction process, and promote the formation of uniform ultrasmall nanoparticles according to the gas-to-particles reaction route [28], [38]. Otherwise, there would be a considerable part of large-size hollow particles in the synthesized nanoparticles that were generated according to the droplets-to-particles reaction route, which would have an unexpected impact on the UCL properties of nanoparticles [28], [38], [39]. To avoid this trouble, the molar ratio of rare-earth-ion cations to 2-EHA is set to 1:3 to ensure that 2-EHA can completely replace nitrate ions. The mixed solution was dispersed by ultrasonic until there was no obvious sediment, and then, the prepared precursor was added into the syringe pump for the swirl-stabilized spray flame reactor to be used in the next step. Y_2O_3:Yb^{3+}/Ho^{3+} UCNPs are synthesized by the self-build swirl-stabilized spray flame reactor, as illustrated in Fig. 1. The reactor composes of two parts which are the swirl-stabilized flame burner and the fine atomization system. The swirl-stabilized flame burner owns eight tangential slits with width in 1 mm and length in 15 mm, in which two groups of non-adjacent slits are used to inject fuel (CH_4, 3 L $\cdot$ min^{-1}) and oxidant (Air, 30 L $\cdot$ min^{-1}), respectively. The swirl number of the burner is 32.72, which is much higher than that required to establish rapid mixed combustion (>5.0), so that the thermal circulation of high-temperature burned gas can form a rapidly mixed combustion area in the outer ring of the reactor [40]. In the swirl flame environment, the fuel and oxidant are injected into the burner respectively, which can greatly eliminate the risk of flashback. The flames generated by adjacent slits can ignite each other to develop a tubular swirl flame, which greatly improves the stability of flame and creates a stable high-temperature environment for the continuous synthesis of large-scale production of UCNPs [28], [40], [41].

The fine atomization system is located at the bottom of the center of the reactor, and the core device of such system is two fluid atomizing nozzles. The precursor liquid was injected into the two fluid atomization nozzles by a syringe pump at a fixed rate of 1200 mL$\cdot$ h^{-1}. At the same time, air with rate of 15 L$\cdot$$min^{-1}$ was injected into the nozzle to atomize the precursor. The precursor was evenly dispersed in the atomized air and gradually developed into an aerosol. The uniformly dispersed aerosol would pass through the pipe like swirl flame and be ignited to form spray flame. Y_2O_3:Yb^{3+}/Ho^{3+} UCNPs would gradually nucleate and grow in the spray flame area and be surged up by the thermal current. An aluminum water-cooled stagnation substrate was adjusted to be directly above the spray flame for the collection of UCNPs. A large temperature gradient will be formed below the water-cooled stagnation substrate, and the synthesized UCNPs will be finally deposited on the lower surface of the substrate through thermophoresis process. Under these conditions, the production rate of UCNPs is $\sim$40 g$\cdot$ h^{-1}, and the production rate can be further improved by increasing the total metal concentration and feed rate of the precursor.

C. Characterization

The crystal morphology and composition of Y_2O_3:Yb^{3+}/Ho^{3+} UCNPs were confirmed by X-ray diffraction (XRD) with Cu K radiation at 40 kV and 50 mA (Rigaku SmartLab SE). The size and morphology of Y_2O_3:Yb^{3+}/Ho^{3+} UCNPs were examined by transmission electron microscopy (TEM, Titan G260-300). For photoluminescence measurements, 2 mg of the prepared sample particles were dispersed in 4 mL ethanol by ultrasonic for 20 minutes. UCNPs were excited by a 980 nm fiber coupled diode laser with a focusing diameter of about 1.5 mm. The UC emission spectra were recorded by a lens coupled grating monochromator (Omnil-l3072i, Zolix) equipped with an integrated photomultiplier tube (PMTH-S1-R928).

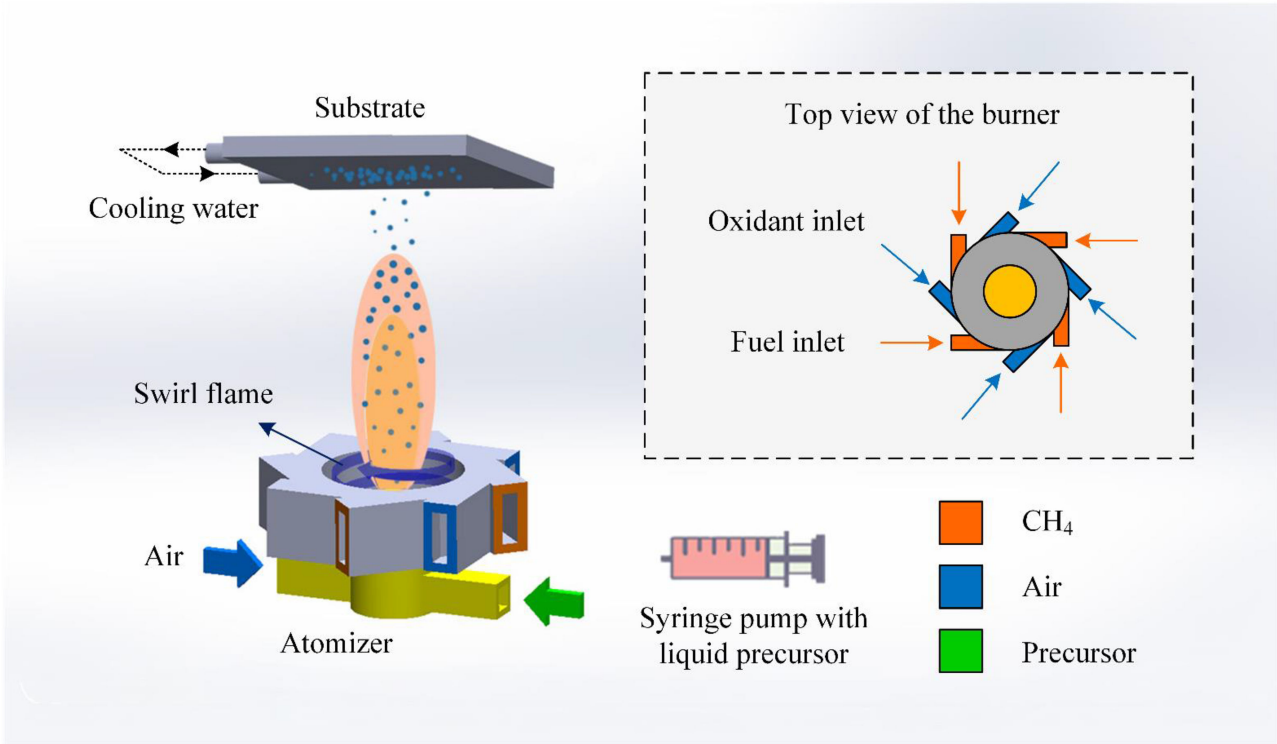

Fig. 1. Schematic of the swirl-stabilized spray flame reactor for large-scale production synthesis of UCNPs.

III. Results and Discussion

A. Structure and Morphology

The crystal phase and morphology characteristics of ultra-small Y_2O_3:Yb^{3+}/Ho^{3+} UCNPs were examined by XRD and TEM. The results are shown in Fig. 2. The XRD patterns of Y_2O_3:Yb^{3+}/Ho^{3+} UCNPs with different doping concentration ratios are shown in Fig. 2(a). From the XRD results, the diffraction peak positions and relative intensities of Y_2O_3:Yb^{3+}/Ho^{3+} UCNPs are consistent with the pure cubic phase Y_2O_3 typical PDF card (JCPDS file No. 86-1107) [28]. With the change of doping concentration, there is no obvious diffraction peak drift or impurity peaks in the XRD spectrum of Y_2O_3:Yb^{3+}/Ho^{3+} UCNPs, indicating that the UCNPs with different doping ratios are highly crystallized and are all pure Y_2O_3 cubic phases. The incorporation of Yb^{3+} and Ho^{3+} ions has a little effect on the crystalline phase of Y_2O_3 nanoparticles.

Fig. 2(b)–(g) present the representative TEM results of Y_2O_3:Yb^{3+}/Ho^{3+} UCNPs, which is consistent with the Y_2O_3 nanoparticles synthesized in other related studies [28], [41]–[45]. Particle size distributions with different doping concentrations are offered inserts of the corresponding TEM images. From the results of particle size distribution, the average size of Y_2O_3:Yb^{3+}/Ho^{3+} UCNPs is ~14 nm. The size of Y_2O_3:Yb^{3+}/Ho^{3+} UCNPs changes little for different doping concentrations, indicating that the doping of Yb^{3+} and Ho^{3+} ions has no obvious effect on the particle size of Y_2O_3 nanoparticles. Significantly, the flame-made Y_2O_3:Yb^{3+}/Ho^{3+} UCNPs are of ~14 nm, which are much smaller than those Y_2O_3 UCNPs made by other methods [10], [30], [31]. The morphology of Y_2O_3 nanoparticles synthesized by flame is mainly determined by its crystalline phase and tends to be non-spherical. This is because the high temperature environment and temperature gradient in the flame reactor make Y_2O_3 nanoparticles be synthesized so rapidly, which leads to the result that the sintering time is shorter than the collision time so that the nanoparticles change from amorphous state to crystalline state [28].

B. UCL Properties

The flame-made Y_2O_3:Yb^{3+}/Ho^{3+} UCNPs were excited by the 980 nm laser to figure out UCL properties. We get the optimal doping concentration (C_{opt}) of flame-made Y_2O_3: Yb^{3+}/Ho^{3+} UCNPs by analyzing the impact of Yb^{3+} and Ho^{3+} doping concentrations. The C_{opt} refers to the doping concentration obtaing the maximal UCL intensity [1]. The power dependence on UCL intensity and the lifetime of such flame-made UCNPs are also discussed in detail.

1) Impact of Yb^{3+} Concentration: To investigate the impact of Yb^{3+} concentration onto the UCL properties of the flame-made Y_2O_3: Yb^{3+}/Ho^{3+} UCNPs and obtain the C_{opt} of Yb^{3+}, a set of Y_2O_3:Yb^{3+}/Ho^{3+} (x/1, x = 1, 2, 4, 6, 8, 10, 15 and 20 mol%) UCNPs were synthesized by SFSP method. Excited by a 980 nm fiber coupled diode laser with a focusing diameter of about 1.5 mm, the spectra of the samples were recorded, as shown in Fig. 3(a). All UCL spectra consist of two major Ho^{3+} emission bands: (1) the green emission band at ~553 nm, assigned as the $^5F_4$, $^5S_2 \rightarrow {}^5I_8$ transitions; (2) the red emission band at ~669 nm, corresponding to the $^5F_5 \rightarrow {}^5I_8$ transition, showing strong green and relatively weak red UCL

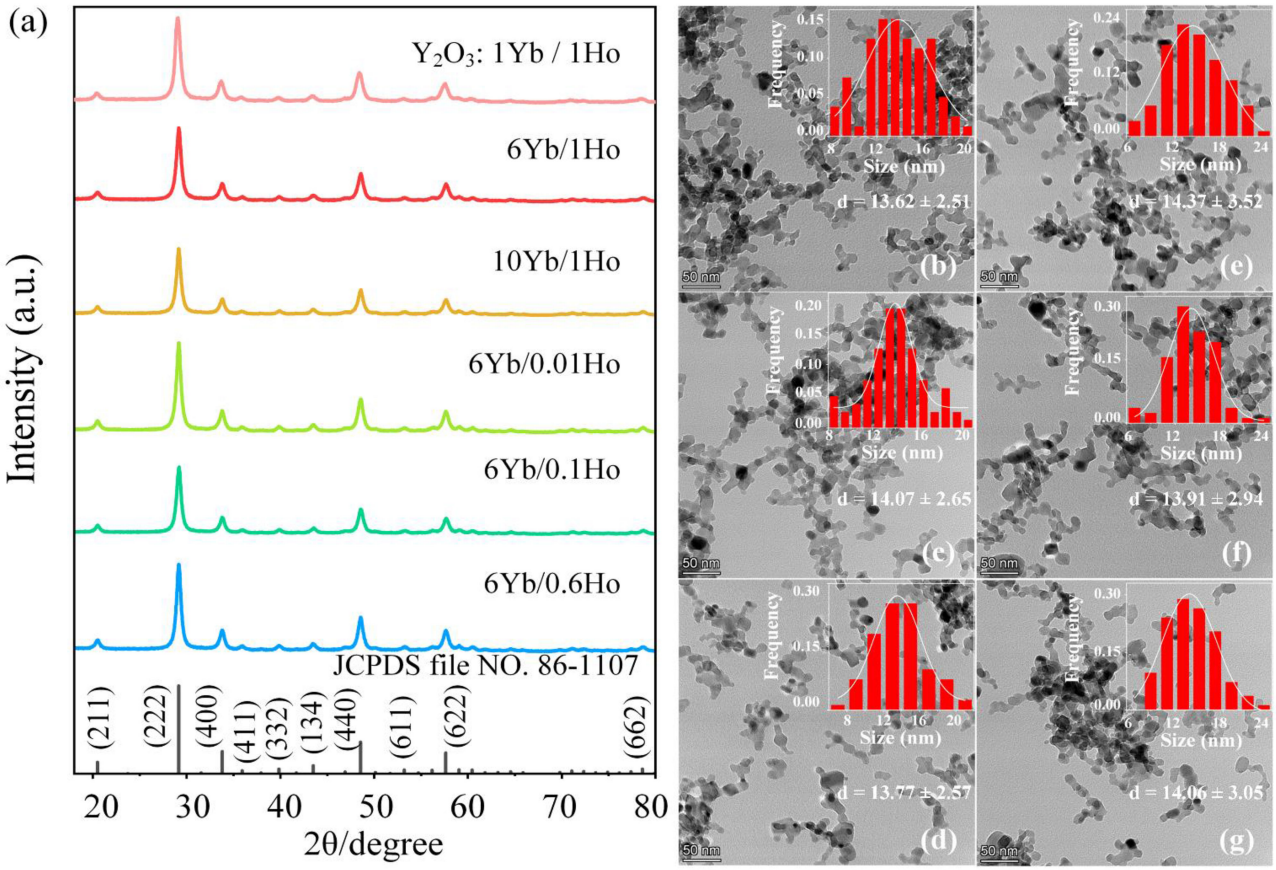

Fig. 2. (a) XRD patterns of Y_2O_3:Yb^{3+}/Ho^{3+} UCNPs with different doping concentration (x/1, x = 1, 6, 10 and 6 / y, y = 0.01, 0.1, 0.6 mol%). TEM images of Y_2O_3:Yb^{3+}/Ho^{3+} UCNPs; (b) Y_2O_3:Yb^{3+}/Ho^{3+} (1/1 mol%); (c) Y_2O_3:Yb^{3+}/Ho^{3+} (6/1 mol%); (d) Y_2O_3:Yb^{3+}/Ho^{3+} (10/1 mol%); (e) Y_2O_3:Yb^{3+}/Ho^{3+} (6/0.01 mol%); (f) Y_2O_3:Yb^{3+}/Ho^{3+} (6/0.1 mol%); (g) Y_2O_3:Yb^{3+}/Ho^{3+} (6/0.6 mol%).

[46]. Due to the reaction environment of high temperature flame, the crystal field surrounding the Yb^{3+} and Ho^{3+} ions in UCNPs were affected, leading vibrational peaks within emission bands broadened and merged with each other so that cannot be seen. We integrated different segments of these spectra, the total, green and red UCL intensities of different Yb^{3+} doping concentration UCNPs were determined and shown in Fig. 3(b). The total UCL intensity of UCNPs was recorded and shown as the orange line with hexagonal icon in Fig. 3(b). According to the orange line, when the Ho^{3+} doping concentration is 1 mol%, the total UCL intensity of UCNPs first enhances with the increase of Yb^{3+} concentration until reaches the maximum at the Yb^{3+} concentration is 6 mol%. After that, the concentration of Yb^{3+} continues to increase and the UCL intensity was gradually weaken. For explanation, when the Yb^{3+} concentration is lower than C_{opt}, the greater number of Yb^{3+} ions will transfer more energy to Ho^{3+} ions, and the UCL efficiency of UCNPs enhances. When the concentration of Yb^{3+} ions exceeds the C_{opt} level, the energy back transfer (EBT) process will gradually become the major part in the UCL process, so that the UCL intensity is gradually weaken [1]. Therefore, it can be considered that the C_{opt} value of Yb^{3+} is 6 mol% under this condition. The other two lines in Fig. 3(b) further confirm that the C_{opt} of Yb^{3+} is equal to 6 mol%, which respectively reflect the green (the green line with circular icon) and red (the red line with diamond icon) UCL intensities as a function of Yb^{3+} concentration, which are of the same rule above. Fig. 3(c) displays the intensity ratio of red and green UCL intensities (R/G ratio) of the samples with different Yb^{3+} concentrations. The R/G ratio of Y_2O_3:Yb^{3+}/Ho^{3+} UCNPs are all lower than 0.5, and it confirms that the UCNPs mainly emit bright green and relatively weak red UCL, the red UCL is much lower than that of green.

2) Impact of Ho^{3+} Concentration: According to the UCL principle of UCNPs, when Ho^{3+} ions work as activators, with the doping concentration gradually increasing from 0 to C_{opt}, the number of luminescence centers increases so that the UCL intensity will gradually increase. When the Ho^{3+} concentration exceeds C_{opt}, owing to the strong interaction between adjacent Ho^{3+} ions, the absorbed excitation energy produces a strong cross-relaxation process between Ho^{3+} ions resulted in fluorescence quenching, so that the UCL intensity of UCNPs decreases with the further increase of Ho^{3+} concentration. To obtain the C_{opt} of Ho^{3+}, another set of Y_2O_3:Yb^{3+}/Ho^{3+} (6/x, x = 0.01, 0.04, 0.08, 0.1, 0.2, 0.4, 0.6, 0.8, 1, 1.5 and 2 mol%) UCNPs was synthesized by SFSP method, and the UCL spectra were also recorded and shown in Fig. 4(a). The two obvious UCL peaks of these spectra are exactly corresponding to the strong green (∼553 nm) and relatively weak red (∼669 nm) UCL.

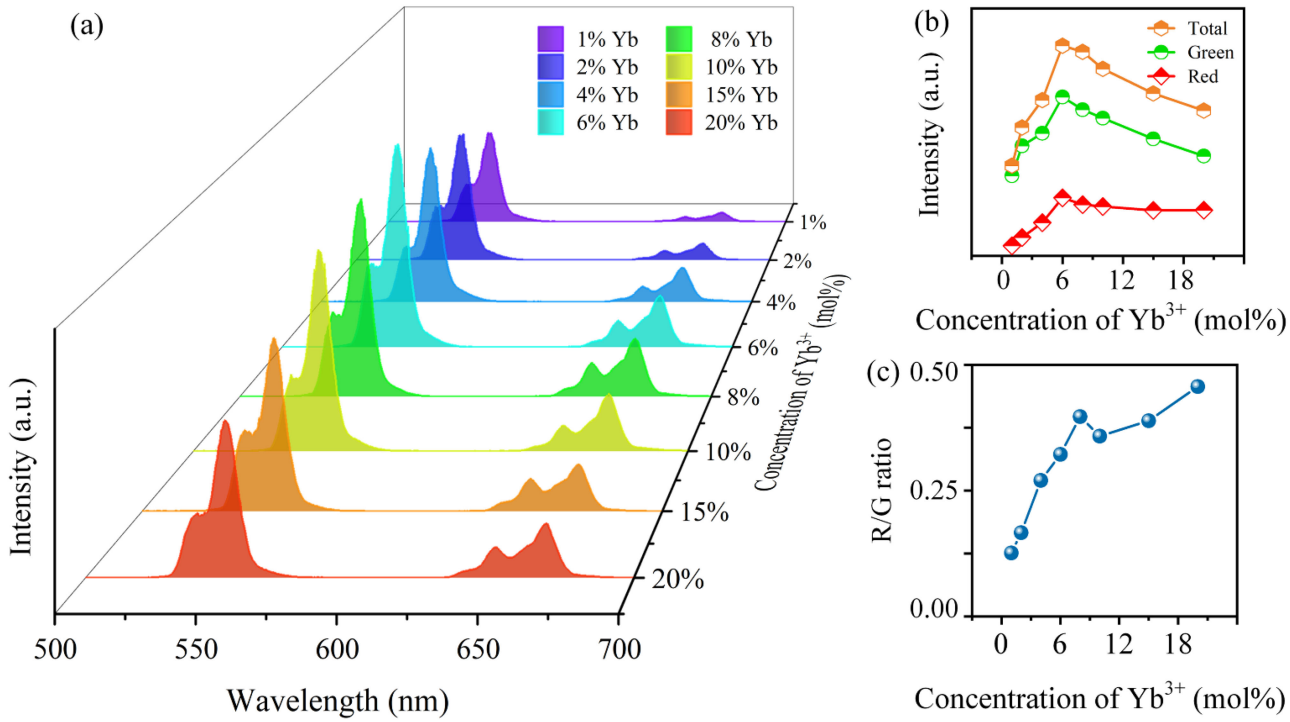

Fig. 3. (a) UCL spectra of Y_2O_3:Yb^{3+}/Ho^{3+} (x/1, x = 1, 2, 4, 6, 8, 10, 15 and 20 mol%) UCNPs at the power density of 565.9 W · cm^{-1}. (b) The intensity of UCL as a function of Yb^{3+} concentration. (c) R/G ratio curve varying with Yb^{3+} concentration.

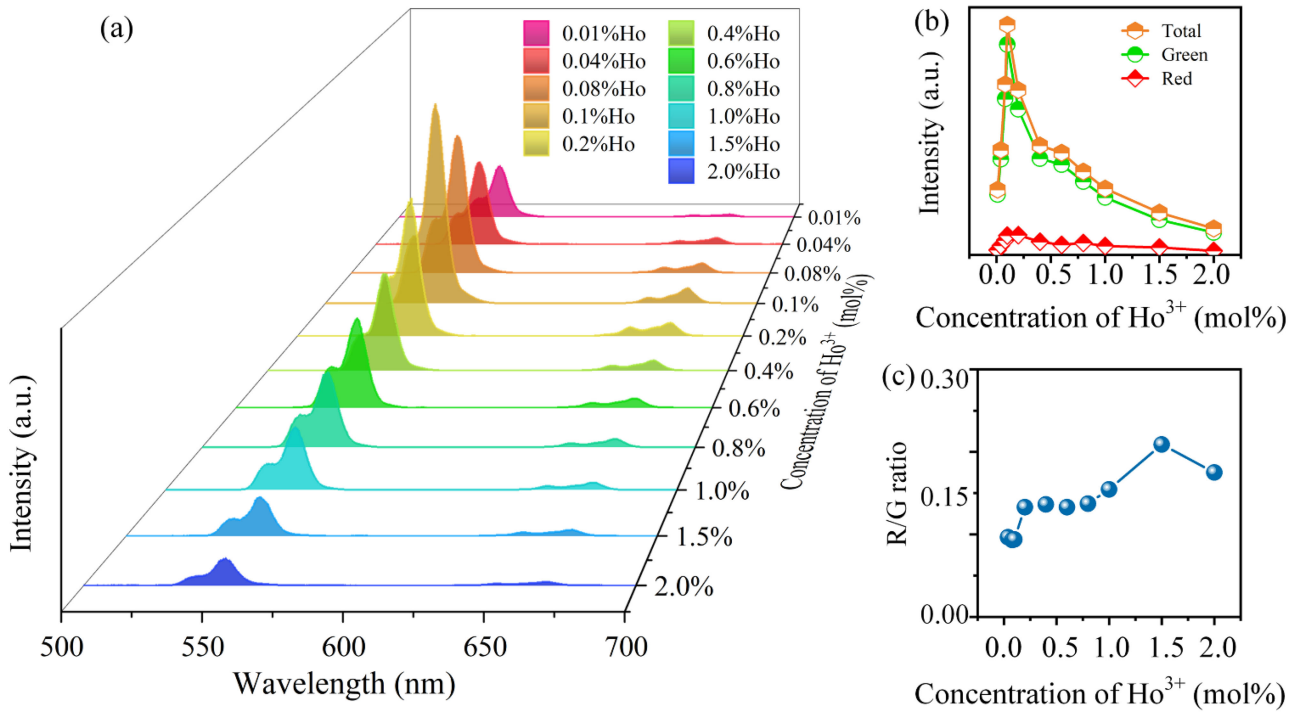

Fig. 4. (a) UCL spectra of Y_2O_3:Yb^{3+}/Ho^{3+} (6/y, y = 0.01, 0.04, 0.08, 0.1, 0.2, 0.4, 0.6, 0.8, 1, 1.5 and 2 mol%) UCNPs at the power density of 565.9 W · cm^{-1}. (b) The intensity of UCL as a function of Ho^{3+} concentration. (c) R/G ratio curve varying with Ho^{3+} concentration.

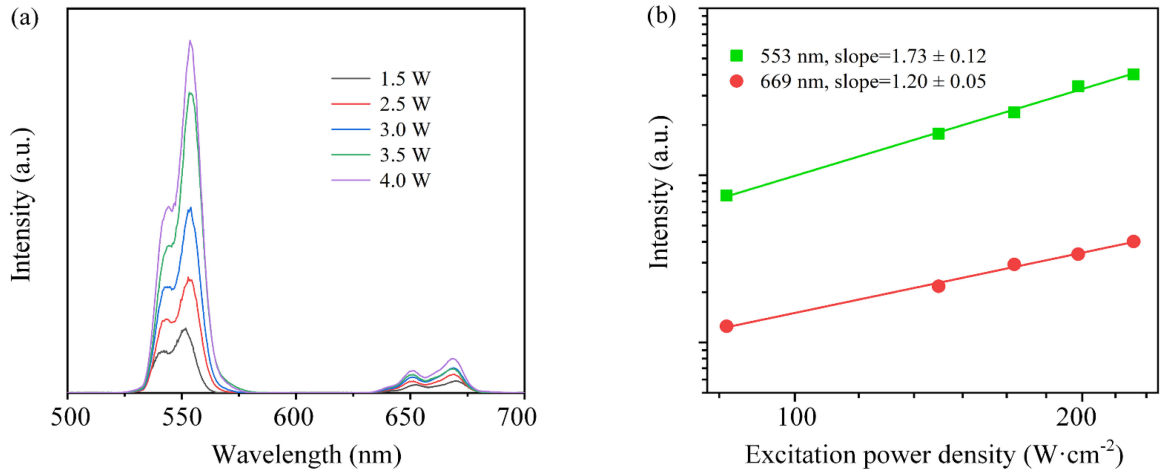

Fig. 5. (a) UCL spectra of Y_2O_3:Yb^{3+}/Ho^{3+} (6/0.1 mol%) UCNPs excited by 980 nm laser with different pump power. (b) Pump power dependence of UCL intensity of Y_2O_3:Yb^{3+}/Ho^{3+} (6/0.1 mol%) UCNPs.

The same method was used to obtain the curves that reflect the relationship between UCL intensity and Ho^{3+} concentration, and the results are shown in Fig. 4(b). The orange line with hexagonal icon in Fig. 4(b) reflects the total UCL intensity as a function of Ho^{3+} concentration. According to the line, when the Yb^{3+} doping concentration is equal to the C_{opt} (6 mol%), the total UCL intensity of UCNPs rapidly enhances to the maximum where the Ho^{3+} concentration is only 0.1 mol%. After that, the UCL intensity decreases fast while the concentration of Ho^{3+} continues to increase. To some extent, this may indicate that the UCL capability of the flame-made Y_2O_3:Yb^{3+}/Ho^{3+} UCNPs is much more sensitive to the doping concentration of Ho^{3+} that compared to the influence of Yb^{3+} concentration. From Fig. 4(b), it is clear that the C_{opt} value of Ho^{3+} is 0.1 mol% under this condition. The C_{opt} level of Ho^{3+} is much lower, because there is a stronger interaction between Ho^{3+} ions so that factors which weaken UCL, like concentration quenching, are easier to occur while the concentration of Ho^{3+} is little higher [1]. The other two lines in Fig. 4(b) are related to the green (the green line with circular icon) and red (the red line with diamond icon) UCL intensities as a function of Ho^{3+} concentration, and they further confirm that the C_{opt} of Ho^{3+} is 0.1 mol% and reflect the same rule. Fig. 4(c) displays the R/G ratio of these samples with different Ho^{3+} concentration. The R/G ratios of Y_2O_3:Yb^{3+}/Ho^{3+} UCNPs are all lower than 0.3, and it means the green UCL accounts for a higher proportion of the total UCL. This indicates that the change of Ho^{3+} concentration shows more impact in green UCL and less in red UCL. Compared to the R/G ratio as the function of Yb^{3+} concentration, the concentration of Ho^{3+} may play a more important role for UCL of Y_2O_3:Yb^{3+}/Ho^{3+} UCNPs.

3) Pump Power Dependence of UCL Intensity: It is well known that there is a nonlinear dependence between UCL intensity (I_{uc}) and laser pump power (P):

$$I_{uc} = \alpha P^n \tag{1}$$

where n is the number of photons required to produce UCL, α is the material correlation coefficient [1]. To further discuss the UCL principle of Y_2O_3:Yb^{3+}/Ho^{3+} UCNPs, the UCL spectra which were excited by the 980 nm laser were measured as a function of pump power, and the sample particles with C_{opt} of Yb^{3+} and Ho^{3+} (6 mol% and 0.1 mol%) were selected for measurement. Fig. 5(a) shows the UCL spectra with the excitation of different laser pump power. From these spectra, it is clear to find that the UCL intensity of nanoparticles gradually enhances with the increase of laser pump power from 1.5 to 4.0 W. Fig. 5(b) shows the linear relations between the UCL intensities at 553 and 669 nm, and laser pump power after taking the logarithm. The slope of the fitting curve reflects the number of photons (n) required for UCL. The n values at 553 and 669 nm are ~1.73 and ~1.20 respectively, which are all between 1 and 2, indicating that the corresponding UCL are all two-photon processes. The experimentally measured value of n is not an integer and the value is smaller than 2, which is because of the cross-relaxation effect in the UC process and the energy loss caused by non-radiative transition [11], [29], [47]. The temperature quenching and thermal damage caused by high-power laser heating will also make n smaller [47]. In addition, the "saturation effect" caused by too high pump power is also the reason for the decrease of measured n.

C. Impact of Synthesis Conditions

The self-build swirl-stabilized spray flame reactor is the key part for our preparation of UCNPs, which is also different to the traditional flame aerosol method. Generally, the speed of inject fuel, oxidant and precursor parameters will mainly affect the establishment of flame condition, and further affect the morphology, size and optical properties of the UCNPs. Therefire, we have further adjusted some synthesized parameters to compare the UCL properties of the obtained Y_2O_3:Yb^{3+}/Ho^{3+} UCNPs. The synthesis conditions are given in Table I. The particle size and production rates of UCNPs are still provided in Table I.

TABLE I
SYNTHESIS CONDITIONS

Conditions	Speed of fuel (L · min^{-1})	Speed of oxidant (L · min^{-1})	Speed of precursor (mL · h^{-1})	Size (nm)	Production rate (g·h^{-1})
A	3	30	1200	13.89 ± 2.23	~40.02
B	3	20	1200	14.10 ± 2.48	~35.40
C	3	25	1200	13.89 ± 2.75	~38.77
D	2.5	30	1200	14.03 ± 2.19	~36.48
E	4	30	1200	13.94 ± 3.51	~37.23
F	3	30	1000	14.17 ± 2.29	~30.14
G	3	30	1400	13.78 ± 2.99	~38.98

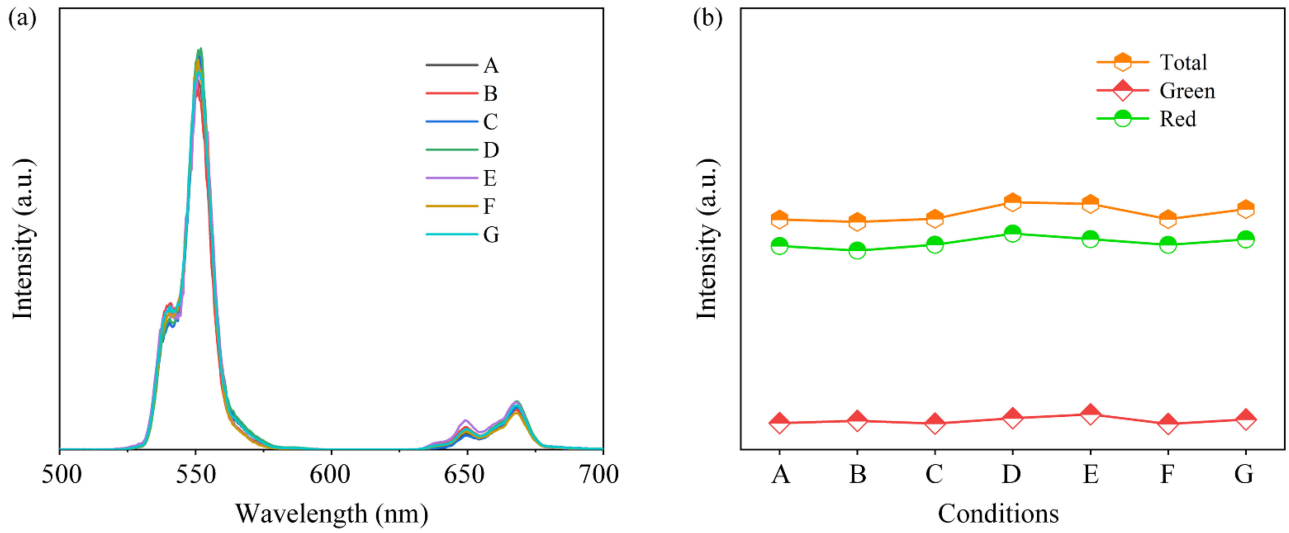

Fig. 6. (a) UCL spectra of UCNPs and (b) intensity comparation of different emission band with condition from A to G.

Fig. 6(a) shows the UCL spectra of UCNPs with different synthesis conditions from A to G and Fig. 6(b) compared their intensities for different UCL. Obviously, the UCL properties remain almost unchanged for Y_2O_3:Yb^{3+}/Ho^{3+} UCNPs fabricated with different synthesis conditions. The UCL properties of flame-made Y_2O_3:Yb^{3+}/Ho^{3+} UCNPs are of high stability, and such a stability is meaningful for large scale industrial production.

Different synthesis conditions mainly affect the production rate of Y_2O_3:Yb^{3+}/Ho^{3+} UCNPs. The production rates with different synthesis conditions are recorded in Table I. The highest production rate was obtained with condition A. The fuel and oxidant are used for building swirl flame, which are used for stabilize the flame environment and ignite the spray flame. When the speed of fuel and oxidant is not appropriate, the stability of combustion will be reduced and production rate reduced accordingly. The speed of precursor is the main parameter to affect production rate of UCNPs, the higher speed of precursor will generally accompany with better production rate, but if the speed is so high that the precursor is not completely atomized, production rate will also be affected.

D. UCL Mechanisms of Y_2O_3:Yb^{3+}/Ho^{3+} UCNPs

The schematic energy level diagram is proposed and shown in Fig. 7. for an in-depth understanding of the UCL mechanism of Y_2O_3:Yb^{3+}/Ho^{3+} UCNPs, The ground state absorption of Ho^{3+}

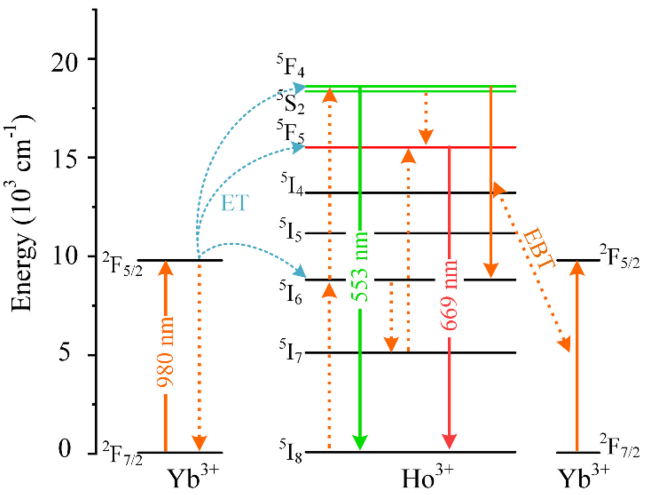

Fig. 7. The energy transfer mechanisms for the UCL process in Y_2O_3:Yb^{3+}/Ho^{3+} UCNPs.

ions by 980 nm laser excitation can be finished with the assist of Yb^{3+} ions. Yb^{3+} ions in the ground state ($^2F_{7/2}$) will absorb excitation energy of 980 nm laser and be transitioned to $^2F_{5/2}$ level ($^2F_{7/2} \rightarrow {}^2F_{5/2}$), and then the excitation energy absorbed by Yb^{3+} ions are transferred to Ho^{3+} ions in $^5I_8$ level to realize ground state absorption process. Phonon assisted non-resonant

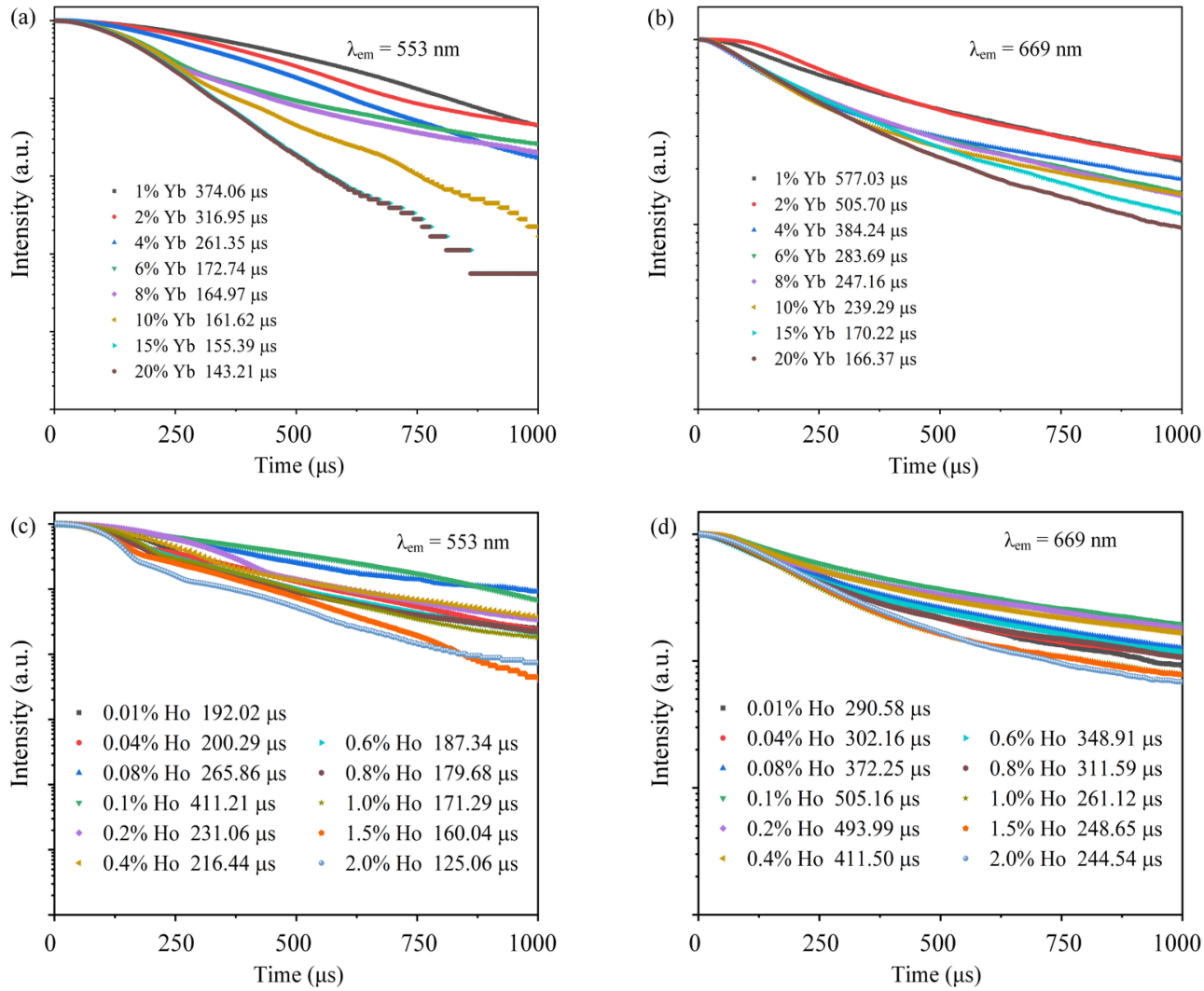

Fig. 8. Decay curves for transition (a) $^5F_4$, $^5S_2 \rightarrow {}^5I_8$ and (b) $^5F_5 \rightarrow {}^5I_8$ of Y_2O_3: Yb^{3+}/Ho^{3+} (x/1 mol%) UCNPs, and transition (c) $^5F_4$, $^5S_2 \rightarrow {}^5I_8$ and (d) $^5F_5 \rightarrow {}^5I_8$ of Y_2O_3: Yb^{3+}/Ho^{3+} (6/x mol%) UCNPs.

energy transfer plays an important role in this process because there is an energy difference of ~1580 cm^{-1} between the $^2F_{5/2}$ level of Yb^{3+} ions and the $^5I_6$ level of Ho^{3+} ions [1].

Ho^{3+} ions in $^5I_8$ level can be transitioned to $^5I_6$ level by the above process. After that, Yb^{3+} ions will return to the ground state and continue to repeat the sensitization process above. Ho^{3+} ions in $^5I_6$ level will then continue to absorb energy from Yb^{3+} ions until be transitioned to $^5F_4$ or $^5S_2$ level ($^5I_6 \rightarrow {}^5F_4$, $^5S_2$). And part of Ho^{3+} ions at $^5F_4$ level or $^5S_2$ level can still further drop to $^5F_5$ level through non-radiative transition process. In addition, Ho^{3+} ions at $^5I_6$ level can still drop to $^5I_7$ level through non-radiative transition process, and then absorb the energy until be transitioned to $^5F_5$ level. Through all the above process, the flame-made Y_2O_3: Yb^{3+}/Ho^{3+} UCNPs will realize the population of upper levels ($^5F_4$, $^5S_2$ and $^5F_5$). Next, Ho^{3+} ions in the upper levels can emit bright green (~553 nm) and relatively weak red (~669 nm) UCL through $^5F_4$, $^5S_2 \rightarrow {}^5I_8$ and $^5F_5 \rightarrow {}^5I_8$ processes, respectively [48], [49]. Moreover, there is a strong EBT: $^5F_4$, $^5S_2$ (Ho^{3+}) + $^2F_{7/2}$ (Yb^{3+}) $\rightarrow$ $^5I_6$ (Ho^{3+}) + $^2F_{5/2}$ (Yb^{3+}) between Yb^{3+} ions and Ho^{3+} ions, which decreased the population of Ho^{3+} ions at $^5F_4$, $^5S_2$ and affected the lifetime of UCL [22], [28].

To further understand the UCL mechanisms, the decay curves of Ho^{3+}: $^5F_4$, $^5S_2 \rightarrow {}^5I_8$ and $^5F_5 \rightarrow {}^5I_8$ transitions under the excitation of 980 nm pulse laser were measured and displayed in Fig. 8. The single exponential function was used to fit the decay curve for obtaining lifetimes of green (553 nm) and red (669 nm) UCL, the results are shown in Fig. 8. It can be clearly seen from Fig. 8(a) and (b) that the lifetime of green UCL exhibits a gradual decline trend as increasing the Yb^{3+} concentration, which drops from 374.06 to 143.21 μs. It is powerful evidence to show the existence of EBT process $^5F_4$, $^5S_2$ (Ho^{3+}) + $^2F_{7/2}$ (Yb^{3+}) $\rightarrow$ $^5I_6$ (Ho^{3+}) + $^2F_{5/2}$ (Yb^{3+}) between Yb^{3+} ions and Ho^{3+} ions [22], [28]. The EBT process will cause depopulation of the $^5F_4$, $^5S_2$ state so that the green UCL lifetime decrease. As the depopulation of the $^5F_4$, $^5S_2$ state, the non-radiative transition process population ($^5F_4$, $^5S_2 \rightarrow {}^5F_5$) decreases and results in the red UCL lifetime showing same decline trend as increasing

TABLE II
ENERGY TRANSFER EFFICIENCY FOR Y_2O_3:Yb^{3+}/Ho^{3+} (x/1 mol %) UCNPS

Yb^{3+} concentration (mol%)	η_{ET} of green UCL (%)
1	40.67
2	49.73
4	58.55
6	72.60
8	73.84
10	74.37
15	75.36
20	77.29

the Yb^{3+} concentration, which drops from 577.03 to 166.37 μs. We still reported the lifetimes of green (553 nm) and red (669 nm) UCL with different Ho^{3+} concentration (Fig. 8(c) and (d)). The lifetime increases while Ho^{3+} concentration is lower than 0.1 mol%, which is exactly the C_{opt} of Ho^{3+}. When the concentration is over than 0.1 mol%, the absorbed excitation energy produces a strong cross-relaxation process between Ho^{3+} ions resulted in fluorescence quenching so that the lifetime decreases [1], [22].

Furthermore, Equation (2) was used for calculating the energy transfer efficiency from Yb^{3+} ions to Ho^{3+} ions [50]:

$$\eta_{ET} = 1 - \frac{\tau_{Yb/Ho}}{\tau_{Ho}} \tag{2}$$

where $\tau_{Yb/Ho}$ and τ_{Ho} are the average lifetime of the transition $^5F_4$, $^5S_2 \rightarrow {}^5I_8$ (669 nm) of Ho^{3+} ions in Y_2O_3:Yb^{3+}/Ho^{3+} (x/1 mol%) UCNPs doped with and without Yb^{3+} ions, respectively. The results are show in Table II. The energy transfer efficiency gradually increases from 40% to 77% as the doping Yb^{3+} ions vary from 1 to 20 mol%. In addition, the quantum yield (QY) was also tested with integrating sphere. The flame-made Y_2O_3:Yb^{3+}/Ho^{3+} UCNPs get the average QY of $\sim$0.162%, which is not too high, and it maybe caused by the ultrasmall particle size. The surface area of the smaller UCNPs which places a higher percentage of the dopant lanthanide ions closer to the surface. This leads to an increase of non-radiative relaxations of the emitting and intermediate levels by solvent molecules and hence an overall decrease in the QY [51].

IV. CONCLUSION

In conclusion, SFSP was firstly used for synthesizing Y_2O_3:Yb^{3+}/Ho^{3+} UCNPs. We successfully fabricated the ultrasmall Y_2O_3:Yb^{3+}/Ho^{3+} UCNPs in a self-build swirl-stabilized spray flame reactor with a high production rate of $\sim$40 g·h^{-1}. Y_2O_3:Yb^{3+}/Ho^{3+} UCNPs synthesized by SFSP shows high UCL stability with different preparation condition, which exactly meet the needs of large-scale industrial production. Excited by 980 nm laser, the synthesized UCNPs emit bright green ($^2F_4$, $^5S_2 \rightarrow {}^2F_{5/2}$) and relatively weak red ($^5F_5 \rightarrow {}^5I_8$) UCL. All these nanoparticles synthesized by SFSP are of cubic phase with an average size of $\sim$14 nm. We still found the C_{opt} of Yb^{3+} and Ho^{3+} in Y_2O_3:Yb^{3+}/Ho^{3+} UCNPs synthesized by SFSP, which are 6 mol% for Yb^{3+} and 0.1 mol% for Ho^{3+}. The UCL spectra of Y_2O_3:Yb^{3+}/Ho^{3+} UCNPs with different conditions were given to confirm these results. In addition, the UCL mechanisms of flame-made Y_2O_3:Yb^{3+}/Ho^{3+} UCNPs were also discussed in detail. Our results suggest that we successfully synthesized ultrasmall Y_2O_3:Yb^{3+}/Ho^{3+} UCNPs by SFSP method, and such method is feasible to achieve large-scale production of continuous one-step synthesis of UCNPs.

ACKNOWLEDGMENT

The authors would like to express gratitude to Professor Li Shuiqing and his team of Tsinghua University for their help in constructing the swirl-stabilized spray flame reactor.

REFERENCES

[1] P. Yang, S. Gai, and F. He, *Rare Earth Upconversion Luminescent Materials*. Beijing, China: Science Press, 2018.
[2] A. Escudero *et al.*, "Rare earth based nanostructured materials: Synthesis, functionalization, properties and bioimaging and biosensing applications," *Nanophotonics*, vol. 6, no. 5, pp. 881–921, 2017.
[3] J. Xiong *et al.*, "Hydrothermal synthesis of $BaLu_2F_8$:Ln^{3+} crystals: Phase/morphology evolution, energy transfer and tunable multicolor luminescence," *CrystEngComm*, vol. 22, no. 29, pp. 4862–4874, 2020.
[4] X. Yang *et al.*, "Simultaneous size manipulation and red upconversion luminescence enhancement of Caf_2:Yb^{3+}/Ho^{3+} nanoparticles by doping with Ce^{3+} ions," *RSC Adv.*, vol. 9, no. 23, pp. 13201–13206, 2019.
[5] W. Gao *et al.*, "Tunable upconversion emission of Ho^{3+}/Yb^{3+}-doped single β-$NaYF_4$ microrod," *Mater. Res. Bull.*, vol. 108, pp. 10–15, 2018.
[6] C. Zhang *et al.*, "A novel scheme to acquire enhanced up-conversion emissions of Ho^{3+} and Yb^{3+} co-doped Sc_2O_3," *Curr. Appl. Phys.*, vol. 20, no. 1, pp. 82–88, 2020.
[7] A. Ali, H. Suo, Y. Wu, J. Xiang, X. Zhao, and C. Guo, "High-purity green emission in Yb^{3+}/Ho^{3+} co-doped $BaIn_6Y_2O_{13}$ up-conversion phosphor," *Ceramics Int.*, vol. 45, no. 7, pp. 8428–8432, 2019.
[8] L. Zhang, G. J. Wang, Y. X. Lu, F. B. Zhang, G. Jia, and C. M. Zhang, "Novel bismuth silicate based upconversion phosphors: Facile synthesis, structure, luminescence properties, and applications," *J. Lumin.*, vol. 216, no. 7, 2019, Art. no. 116718.
[9] P. K. Vishwakarma, S. B. Rai, and A. Bahadur, "Intense red and green emissions from Ho^{3+}/Yb^{3+} co-doped dodium gadolinium molybdate nano-phosphor: Effect of calcination temperature and intrinsic optical bistability," *Mater. Res. Bull.*, vol. 133, no. 11, 2021, Art. no. 111041.
[10] F. L. Chawarambwa *et al.*, "Synthesis of Yb^{3+}/Ho^{3+} co-doped Y_2O_3 nanoparticles and its application to dye sensitized solar cells," *J. Mol. Struct.*, vol. 1228, no. 15, 2021, Art. no. 129479.
[11] G. B. Nair, A. Kumar, H. C. Swart, and S. J. Dhoble, "Facile precipitation synthesis of green-emitting Bay_2F_8:Yb^{3+}, Ho^{3+} upconverting phosphor," *Ceramics Int.*, vol. 45, no. 11, pp. 14205–14213, 2019.
[12] T. X. Gu *et al.*, "Upconversion composite nanoparticles for tumor hypoxia modulation and enhanced near-infrared-triggered photodynamic therapy," *ACS Appl. Mater. Inter.*, vol. 10, no. 18, pp. 15494–15503, 2018.
[13] Q. Y. Huang, W. H. Ye, X. F. Jiao, L. L. Yu, Y. L. Liu, and X. T. Liu, "Efficient upconversion fluorescence in $NaYF_4$: Yb^{3+}, Er^{3+}/m$NaYF_4$ multilayer core-shell nanoparticles," *J. Alloys Compounds*, vol. 763, pp. 216–222, 2018.
[14] Y. Song *et al.*, "Synthesis and inkjet printing of NaYF4:Ln^{3+}@$NaYF_4$ core-shell nanoparticles with enhanced upconversion fluorescence for anti-counterfeiting applications," *J. Nanoscience Nanotechnol.*, vol. 20, no. 3, pp. 1511–1519, 2020.
[15] H. L. Jiang *et al.*, "Preparation and upconversion properties of rare earth doped core-shell $Y(OH)_3$ and β-$NaYF_4$ hybrid nanorods," *Mater. Res. Bull.*, vol. 101, pp. 61–66, 2018.
[16] F. Zhang *et al.*, "Mesoporous multifunctional upconversion luminescent and magnetic 'nanorattle' materials for targeted chemotherapy," *Nano Lett.*, vol. 12, no. 1, pp. 61–67, 2012.
[17] Z. Liu, H. W. Deng, and D. H. Chen, "Temperature dependent upconversion properties of Yb^{3+}: Ho^{3+} co-doped Gd_2O_3 nanoparticles prepared by pulsed laser ablation in water," *Ceramics Int.*, vol. 45, no. 10, pp. 13235–13241, 2019.
[18] R. Anjana, T. K. Krishnapriya, and M. K. Jayaraj, "Clean synthesis of Er, Yb doped fluorapatite upconversion luminescent nanoparticles through liquid phase pulsed laser ablation," *Opt. Laser Technol.*, vol. 131, 2020, Art. no. 106452.
[19] P. F. Shuai, L. B. Liao, Q. F. Guo, D. Yang, R. Q. Shi, and L. F. Mei, "Preparation and up-conversion luminescence characteristics studies of K_3YF_6: Ho^{3+}, Yb^{3+} with cryolite structure," *J. Lumin.*, vol. 236, 2021, Art. no. 118104.

[20] Y. Mu, P. Du, W. Li, and L. Luo, "A photochromism induced dual-mode luminescence modulation in SR_2SnO_4:XYb^{3+}/Ho^{3+} ceramics," *Ceramics Int.*, vol. 47, no. 17, pp. 25037–25044, 2021.

[21] Q. Xiao *et al.*, "Tunable multicolor upconversion luminescence of Yb^{3+} sensitized $Na_3La(VO_4)_2$ crystals," *J. Amer. Ceram. Soc.*, vol. 104, no. 3, pp. 1415–1423, 2020.

[22] S. Liu *et al.*, "Intense upconversion luminescence and energy-transfer mechanism of Ho^{3+}/Yb^{3+} co-doped $SrLu_2O_4$ phosphor," *J. Amer. Ceram. Soc.*, vol. 100, no. 8, pp. 3530–3539, 2017.

[23] L. Zhang *et al.*, "Facile synthesis, structure, and tunable luminescence properties of novel one-dimensional $Bi_4Si_3O_{12}$ fibers," *CrystEngComm*, vol. 22, no. 11, pp. 2002–2012, 2020.

[24] X. Wang *et al.*, "Up-conversion photoluminescence properties and energy transfer process of Ho^{3+}, Yb^{3+} co-doped BaY_2F_8 fine fibers," *J. Lumin.*, vol. 212, pp. 154–159, 2019.

[25] G. A. Kelesidis, E. Goudeli, and S. E. Pratsinis, "Flame synthesis of functional nanostructured materials and devices: Surface growth and aggregation," *Proc. Combustion Inst.*, vol. 36, no. 1, pp. 29–50, 2017.

[26] B. Schimmoeller, S. E. Pratsinis, and A. Baiker, "Flame aerosol synthesis of metal oxide catalysts with unprecedented structural and catalytic properties," *ChemCatChem*, vol. 3, no. 8, pp. 1234–1256, 2011.

[27] S. E. Pratsinis, "Aerosol-based technologies in nanoscale manufacturing: From functional materials to devices through core chemical engineering," *AIChE J.*, vol. 56, no. 12, pp. 3028–3035, 2010.

[28] X. Yang *et al.*, "Flame-made Y_2O_3:Yb^{3+}/Er^{3+} upconversion nanoparticles: Mass production synthesis, multicolor tuning and thermal sensing studies," *J. Alloys Compounds*, vol. 854, no. 28, 2021, Art. no. 157078.

[29] N. An, L. H. Ye, R. J. Bao, L. H. Yue, and L. G. Wang, "Up-conversion luminescence characteristics and temperature sensing of Y_2O_3: Ho_3+/Yb_3+ single crystal fiber," *J. Lumin.*, vol. 215, no. 6, 2019, Art. no. 116657.

[30] S. H. Huang *et al.*, "Rapid, morphologically controllable, large-scale synthesis of uniform $Y(OH)_3$ and tunable luminescent properties of Y_2O_3:Yb^{3+}/Ln^{3+} (Ln = Er, Tm and Ho)," *J. Mater. Chem.*, vol. 22, no. 31, pp. 16136–16144, 2012.

[31] Q. Lu, A. Li, F. Guo, L. Sun, and L. Zhao, "Experimental study on the surface modification of Y_2O_3:Tm^{3+}/Yb^{3+} nanoparticles to enhance upconversion fluorescence and weaken aggregation," *Nanotechnology*, vol. 19, no. 14, 2008, Art. no. 145701.

[32] S. H. Guo, X. J. Xie, L. Huang, and W. Huang, "Sensitive water probing through nonlinear photon upconversion of lanthanide-doped nanoparticles," *ACS Appl. Mater. Interfaces*, vol. 8, no. 1, pp. 847–853, 2016.

[33] J. Dong *et al.*, "Tuning and enhancing the red upconversion emission of Er^{3+} in $LiYF_4$ nanoparticles," *J. Lumin.*, vol. 207, pp. 361–368, 2019.

[34] M. H. Alkahtani, C. L. Gomes, and P. R. Hemmer, "Engineering water-tolerant core/shell upconversion nanoparticles for optical temperature sensing," *Opt. Lett.*, vol. 42, no. 13, pp. 2451–2454, 2017.

[35] C. V. Ramana, V. H. Mudavakkat, K. K. Bharathi, V. V. Atuchin, L. D. Pokrovsky, and V. N. Kruchinin, "Enhanced optical constants of nanocrystalline yttrium oxide thin films," *Appl. Phys. Lett.*, vol. 98, no. 3, 2011, Art. no. 031905.

[36] V. H. Mudavakkat, V. V. Atuchin, V. N. Kruchinin, A. Kayani, and C. V. Ramana, "Structure, morphology and optical properties of nanocrystalline yttrium oxide (Y_2O_3) thin films," *Opt. Mater.*, vol. 34, no. 5, pp. 893–900, 2012.

[37] T. L. Zhao *et al.*, "Synthesis and up-conversion luminescence properties of Ho^{3+}-Yb^{3+} co-doped glass ceramics containing $Sr_3Gd(PO_4)_3$," *Opt. Mater.*, vol. 121, no. 8, 2021, Art. no. 111547.

[38] S. Li, Y. Ren, P. Biswas, and S. D. Tse, "Flame aerosol synthesis of nanostructured materials and functional devices: Processing, modeling, and diagnostics," *Prog. Energy Combustion Sci.*, vol. 55, pp. 1–59, 2016.

[39] J. L. Wei, S. Q. Li, Y. H. Ren, Y. Y. Zhang, and S. D. Tse, "Investigating the role of solvent formulations in temperature-controlled liquid-fed aerosol flame synthesis of YAG-based nanoparticles," *Proc. Combustion Inst.*, vol. 37, no. 1, pp. 1193–1201, 2019.

[40] J. L. Wei, Y. H. Ren, Y. Y. Zhang, B. L. Shi, and S. Q. Lia, "Effects of temperature-time history on the flame synthesis of nanoparticles in a swirl-stabilized tubular burner with two feeding modes," *J. Aerosol Sci.*, vol. 133, pp. 72–82, 2019.

[41] X. F. Zhao *et al.*, "Dual-wavelength excited intense red upconversion luminescence from Er^{3+}-sensitized Y_2O_3 nanocrystals fabricated by spray flame synthesis," *Nanomaterials*, vol. 10, no. 8, 2020, Art. no. 1475.

[42] A. Camenzind, R. Strobel, F. Krumeich, and S. E. Pratsinis, "Luminescence and crystallinity of flame-made Y_2O_3: Eu^{3+} nanoparticles," *Adv. Powder Technol.*, vol. 18, no. 1, pp. 5–22, 2007.

[43] R. Kubrin, A. Tricoli, A. Camenzind, S. E. Pratsinis, and W. Bauhofer, "Flame aerosol deposition of Y_2O_3: Eu nanophosphor screens and their photoluminescent performance," *Nanotechnology*, vol. 21, no. 22, 2010, Art. no. 225603.

[44] G. A. Sotiriou, M. Schneider, and S. E. Pratsinis, "Color-tunable nanophosphors by codoping flame-made Y_2O_3 with Tb and Eu," *J. Phys. Chem. C*, vol. 115, no. 4, pp. 1084–1089, 2011.

[45] G. A. Sotiriou, M. Schneider, and S. E. Pratsinis, "Green, silica-coated monoclinic Y_2O_3:Tb^{3+} nanophosphors: Flame synthesis and characterization," *J. Phys. Chem. C*, vol. 116, no. 7, pp. 4493–4499, 2012.

[46] V. Kumar, B. Zoellner, P. A. Maggard, and G. Wang, "Effect of doping ge into Y_2O_3:Ho,Yb on the green-to-red emission ratio and temperature sensing," *Dalton Trans.*, vol. 47, no. 32, pp. 11158–11165, Aug. 2018.

[47] B. P. Kore *et al.*, "Spectroscopic investigation of up-conversion properties in green emitting $BaMgF_4$:Yb^{3+}, Tb^{3+} phosphor," *Inorganic Chem.*, vol. 56, no. 9, pp. 4996–5005, 2017.

[48] D. Li *et al.*, "Enhanced upconversion emission and magnetization in $Yb3+$-Er^{3+}/Ho^{3+} codoped Gd_2O_3 nanocrystals by introducing Zn^{2+} ions," *J. Alloys Compounds*, vol. 675, pp. 31–36, 2016.

[49] C. S. Lim, A. Aleksandrovsky, V. Atuchin, M. Molokeev, and A. Oreshonkov, "Microwave-employed Sol–Gel synthesis of scheelite-type microcrystalline $AgGd(MOO_4)_2$:Yb^{3+}/Ho^{3+} upconversion yellow phosphors and their spectroscopic properties," *Crystals*, vol. 10, no. 11, 2020, Art. no. 1000.

[50] M. Azam and V. K. Rai, "Enhanced frequency upconversion in Er_{3+}-Yb_{3+} codoped heavy metal oxides based tellurite glasses," *Methods Appl. Fluorescence*, vol. 6, no. 2, Jan. 2018, Art. no. 025002.

[51] J. C. Boyer and F. C. van Veggel, "Absolute quantum yield measurements of colloidal $NaYF_4$: Er^{3+}, Yb^{3+} upconverting nanoparticles," *Nanoscale*, vol. 2, no. 8, pp. 1417–1419, Aug. 2010.